# Elaboration and characterization of hydrogen standard stable under heavy ion irradiation: application to nuclear astrophysics

Genard, Gilles; Yedji, Mourad; Ross, Guy G.; Terwagne, Guy

*Published in:*
Nuclear Instruments and Methods in Physics Rresearch B

*Publication date:*
2007

*Document Version*
Early version, also known as pre-print

Available online at www.sciencedirect.com
ScienceDirect
Nuclear Instruments and Methods in Physics Research B 264 (2007) 156–164
NIM B
Beam Interactions with Materials & Atoms
www.elsevier.com/locate/nimb

# Elaboration and characterization of hydrogen standard stable under heavy ion irradiation: Application to nuclear astrophysics

G. Genard [a,*], M. Yedji [b], G.G. Ross [b], G. Terwagne [a]

[a] *Laboratoire d'Analyses par Réactions Nucléaires, FUNDP – University of Namur, 61 Rue de Bruxelles, B-5000 Namur, Belgium*
[b] *INRS-Energie, Matériaux et Télécommunications, 1650 Boulevard Lionel-Boulet, Varennes, Québec, Canada J3X 1S2*

Received 24 January 2007; received in revised form 20 July 2007
Available online 19 August 2007

**Abstract**

A hydrogen standard has been carried out by ion implantation in silicon. The silicon wafer was implanted with hydrogen at different energies and fluences to provide a ~100 nm flat distribution to the specimen. The samples obtained were characterized by mean of elastic recoil detection analysis (ERDA) and resonant nuclear reaction analysis (RNRA). All important properties of the hydrogen standard have been controlled: isotopic purity, depth profile, stability under ion irradiation and reproducibility. The standards were validated by the measurement of the resonant cross-section of the $^{13}C(p,\gamma)^{14}N$ reaction. The similarity of the resonance energy, the resonance width and the resonance strength measurements with those reported in literature confirms the validity of the proposed procedure for hydrogen standards. Therefore, this kind of target could be used to investigate all nuclear reactions in which a proton is involved, from reactions with astrophysical interest to the ones with concern in material analysis.


*PACS:* 25.40.Lw; 25.40.Ny; 25.60.Dz

*Keywords:* Hydrogen standard; Ion implantation; Silicon; Cross-section; Nuclear astrophysics

## 1. Introduction

Hydrogen plays an important role in material engineering. The lighter element of the Mendeleyev table but the most abundant in the universe can for example modify metal properties such as embrittlement and corrosion [1]. Hydrogen is essential in many other fields. For instance, in chemistry, hydrogen is omnipresent in the context of the development of new polymers with extraordinary properties (biocompatibility, light emission, active polymers, etc). In electronics, microchips, tending to nanochips, can now be produced by use of the Smart Cut™ process involving hydrogen implantation in silicon [2–5]. This element is also appreciated in optics, where it is used to improve the optical properties of silicon nanocrystals, a very popular emerging technology aiming at the development of a silicon laser, by means of hydrogen passivation [6]. At a more fundamental level, the double helix of DNA exists thanks to hydrogen bonding interactions.

Due to the multiple applications involving hydrogen, it is important to develop and/or refine powerful techniques that can be used to characterize this element in materials. This can be done with nuclear reactions that are well known to be non destructive and quantitative, the latter necessitating the knowledge of reaction cross-sections. The precise measurement of nuclear cross-sections requires the use of a reference standard of known concentration of the element on which the reaction of interest is done.

The need for known cross-sections and thus of standards is largely justified by the requirement in industry to understand and exploit material properties but is also essential for more fundamentals studies. For example, to profile nitrogen in steel the $^{14}N(^{3}He,p)^{16}O$ and $^{14}N(^{3}He,\alpha)^{13}N$ reactions

* Corresponding author. Tel.: +32 81 72 5479; fax: +32 81 72 5473.
*E-mail address:* gilles.genard@fundp.ac.be (G. Genard).

0168-583X/$ - see front matter © 2007 Elsevier B.V. All rights reserved.
doi:10.1016/j.nimb.2007.08.007

are used [7]. Another example is the $^{19}F(p,\alpha\gamma)^{16}O$ reaction, with a resonance at 340 keV, that is sensitive to fluorine present in teeth [8]. A standard is also required for the measurement of cross-sections such as that of the elastic recoil reaction $^{1}H(^{3}He,^{1}H)^{3}He$ [9].

In addition to the preceding considerations, there is an astrophysical interest in realizing a hydrogen standard. Stars, such as our sun, are mostly composed of hydrogen (75%) and helium (25%). Energy production is mainly governed by thermonuclear reactions occurring in stars. To understand their evolution, it is necessary to determine the reaction rate of the different reactions involved. That can be achieved from the cross-sections that are usually measured in laboratories by nuclear physicists. Among the reactions of interest are all the ones in which a proton is involved. They can quote for instance the p–p chain or the CNO cycle. The p–p chain, the dominant energy production process in our sun, presents some interesting proton induced reactions that are still under investigation as the $^{2}H(p,\gamma)^{3}He$ reaction [10]. The CNO cycle, first described by Hans Bethe in 1939 [11], dominates the energy production for stars heavier than 2 solar masses during the hydrogen combustion phase. Inside the cold CNO cycle (for temperature below $0.2 \times 10^{9}$ K), the slowest and most important reaction, $^{14}N(p,\gamma)^{15}O$, has been largely studied by irradiating a target of $^{14}N$ with protons and detecting the outgoing gamma rays [12–15]. However, this procedure can lead to artifacts because of the nuclear reaction of protons with impurities always present in the targets used. Thus, there are many advantages of working in reverse kinematics, which means, for instance, irradiating a target containing hydrogen with ions of $^{14}N$ as proposed in this work. The need of stable and reliable hydrogen standard is then shown.

Another interesting reaction of the (cold) CNO cycle is the $^{13}C(p,\gamma)^{14}N$ reaction. In addition, this reaction plays a major role in production of elements heavier than iron in asymptotic giant branch (AGB) stars. Indeed, this stellar environment contains helium and $^{12}C$ in a hydrogen burning shell where the following process can take place: $^{12}C(p,\gamma)^{13}N(\beta^{+})^{13}C(\alpha,n)^{16}O$. The $^{13}C(\alpha,n)^{16}O$ is a major neutron source, necessary in the s-process. This reaction is in competition with the $^{13}C(p,\gamma)^{14}N$ reaction. Therefore, the more the reaction rate of the $^{13}C(p,\gamma)^{14}N$ reaction is important, the more the number of available neutrons for the s-process is low. The knowledge of this reaction is also important if one is investigating the $^{13}N(p,\gamma)^{14}O$ because the $^{13}N$ and $^{13}C$ masses are nearly the same and cannot be separated in a beam. It is thus necessary to subtract the contribution of $^{13}C$ in the gamma rays spectra, as discussed by Galster et al. [16].

The $^{13}C(p,\gamma)^{14}N$ reaction presents a resonance due to the presence of an excited level of $^{14}N$ at 8.062 MeV, which can be reached by providing an energy of 511 keV in the $^{13}C + p$ centre of mass system, as pointed out on Fig. 1. We have chosen to measure the cross-section around this 511 keV resonance. On the one hand, it is a good test case

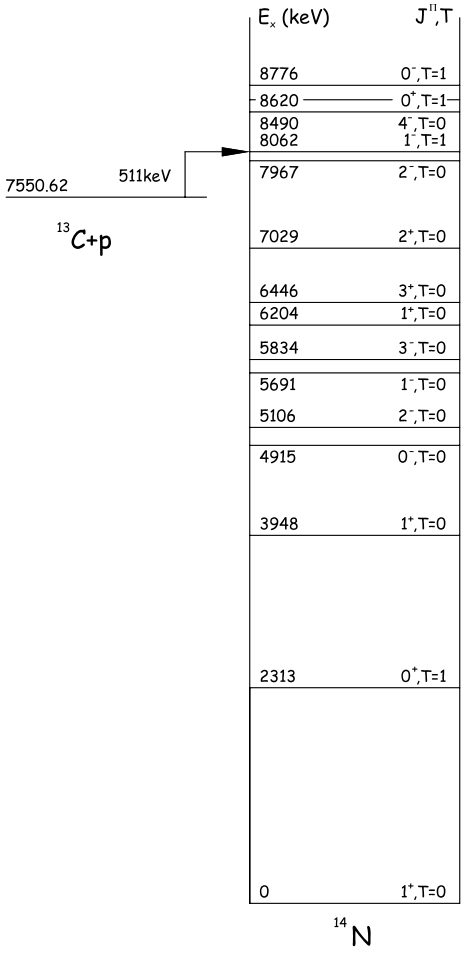


Fig. 1. $^{14}N$ energy level scheme [17]. The resonant level at 8062 keV is underlined from the $^{13}C + p$ level. The parity, spin and isospin of the different levels are given.

for the hydrogen standard. On the other hand, this reaction has a higher cross-section than $^{14}N(p,\gamma)^{15}O$ and could be a suitable reaction with astrophysical interest as a first investigation. The data for the S-factor at the resonance energies given in NACRE[1] [18] are essentially from the article of King et al. [19]. At lower energies, the S-factor is dominated by the tail of the 511 keV resonance and it exists some discrepancies with high error bars around 150 keV for instance, as shown in Fig. 2 that is taken from NACRE. This figure gives the S-factor in function of the temperature occurring in the star $T_9$ (in billion Kelvin) or in function of the corresponding energy in the center of mass system E. In this figure, the solid line is an extrapolation to energies not accessible experimentally, obtained from a numerical treatment, using the available data. Additional data would be very useful to improve the knowledge of the S-factor value at very low energies. In [16], they gave a review on the different measurements of this resonance [19–23] and they checked off a resonance width in the range of 30–37 keV which is rather indefinite. So there are still reasons to study

[1] Nucler Astrophysics Compilation of REaction Rates.

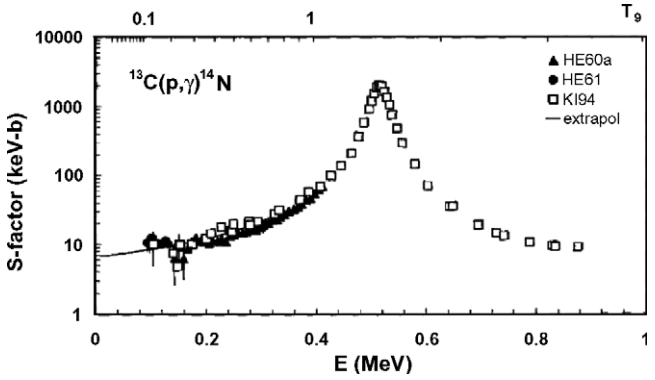


Fig. 2. S-factor of the $^{13}C(p,\gamma)^{14}N$ reaction taken from NACRE [18], showing the low number of reference data and the high discrepancies around 150 keV.

it in reverse kinematics by using a hydrogen standard. The ALTAÏS[2] accelerator installed at LARN is the ideal machine to take up this challenge. The energy covered by this accelerator overlap the 511 keV resonance with a very good energy resolution (~200 eV).

To obtain a good standard, two challenges must be mastered. The first one is the fact that the standard will be irradiated with a heavy ion beam, which could induce hydrogen desorption [24]. The second difficulty comes from the necessary isotopic purity of the $^1H$ standard. It is extremely important to make sure that no deuterium is incorporated in the standard because nuclear reactions with deuterium have generally much higher cross-sections and can interfere and even completely mask the nuclear reactions on $^1H$. The latter are reactions which are of interest in the above mentioned studies. Hence, we had to carefully verify that no deuterium falsifies the cross-section measurements. These two challenges can be overcome by producing the standard by implantation of hydrogen ions in silicon. On the one hand, the implantation with mass separation makes sure that no deuterium is implanted in the material and, on the other hand, the stability under irradiation of hydrogen implanted into silicon is well known [25]. It is due to the strong binding of the hydrogen atoms with silicon defects (such as $V_2H_6$) created during the implantation and the H-terminated internal surfaces Si(1 0 0) [26–28].

Ideally, the standard should exhibit a flat and thin hydrogen depth profile with a hydrogen concentration as high as possible and starting from the very first nanometers. A hydrogen profile thickness of 100 nm is a good compromise between the intensity of the detected gamma signal and the precision in the cross-section measurement. These characteristics can be achieved with implantation energies in the range of a few keV, which is easily obtained with our implanters.

The $^{15}N(p,\alpha\gamma)^{12}C$ nuclear reaction will be used to precisely determine the hydrogen depth profile in the standard [29,30], while elastic recoil detection analysis (ERDA) will serve to verify the isotopic purity. Details will be given in the experimental section.

[2] Accélérateur Linéaire Tandetron pour l'Analyse et l'Implantation des Solides.

## 2. Experimental details

### 2.1. Hydrogen implantation into silicon

The silicon samples were implanted by means of two ion implanters. The first one makes use of a Wien filter for the ion mass selection, which is the application of crossed electric and magnetic fields ($E \times B$) with an ion deviation of 3° to reject the neutral particles. The second implanter is equipped with a magnetic field that selects the ion mass with a deviation angle of 20°. This implanter allows very good mass separation. The ideal procedure to obtain the hydrogen standard is to implant $^1H^+$ as ion species, rather than $^1H_2^+$, to avoid deuterium implantation, which has nearly the same mass. However, for preliminary studies, for which isotopic purity is not necessary, $^1H_2^+$ ions were implanted for easiness. All implantations were done at room temperature.

For the study of the evolution of the retained dose as a function of the incident fluence, 3 keV $^1H_2^+$ ions were implanted. The integrated hydrogen depth profiles were measured by the ERD ExB method, using a 350 keV $^4He$ beam, described in detail in [31].

In a second step, two successive implantations of $^1H^+$ at different energies (3 and 1.5 keV), were carried out in order to obtain a homogeneous hydrogen concentration to a depth of 100 nm. The implantation energies were determined by means of SRIM [32] simulations, which give projected ranges of 30 nm and 50 nm for $^1H^+$ energies of 1.5 keV and 3 keV, respectively. The energy loss by $^{13}C$ ions of 7.2 MeV in such a hydrogen standard is about 100 keV, which corresponds to the energy steps for the cross-section measurement.

Finally, to differentiate the implanted hydrogen and the surface contribution due to contamination, some implantations of $^1H^+$ were performed at higher energy (24 keV) by means of a 150 kV SAMES accelerator equipped with magnetic deflection.

### 2.2. Hydrogen and deuterium depth profiling

All analyses, except the measurements of the retained dose, were done with ALTAÏS, the linear accelerator installed at LARN. It is a tandetron with a 2 MV terminal high voltage which allows acceleration of nearly all negative ions produced either by a source of negative ions by cesium sputtering (SNICS) or by a duoplasmotron gas source.

Using the appropriate reaction, we are sensitive to hydrogen and deuterium, and can thus verify the isotopic purity of the standard. Indeed, elastic recoil detection analysis (ERDA) gives some interesting information, such as the depth profile and the ion dose of hydrogen and

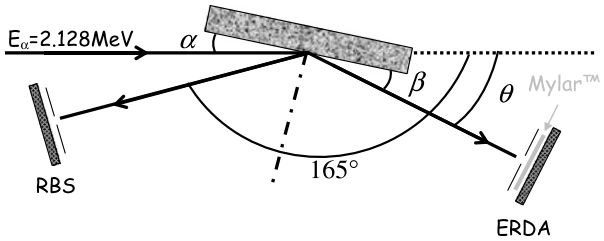


Fig. 3. Principle diagram of ERD geometry: $\alpha$ and $\beta$ are respectively the incident and detection angles and $\theta$ the recoil angle of the two hydrogen isotopes. The RBS detector placed at 165° relative to the incident beam is used as a monitor.

deuterium simultaneously. To produce these recoils, 2.128 MeV alpha particles were used to benefit from the presence of an intense resonance on deuterium, with an increasing cross-section for the lowest recoil angles [33]. Therefore, in order to be very sensitive to deuterium, we have chosen, relatively to the Fig. 3, $\alpha = 15°$ and $\beta = 5°$. So the recoil angle, $\theta$, was 20°, providing a cross-section on deuterium 75 times higher than the Rutherford cross-section. A Mylar™ foil was placed in front of the ERD detector to stop the backscattered alpha particles. On the other hand, a RBS detector was located at 165°, relative to the incident beam, in order to monitor the incoming ion flux by detecting the spectrum of the alpha particles backscattered from the silicon matrix. The particles were detected in two PIPS[3] detectors. To take into account the high angular sensitivity of the technique, a rectangular slit of $1 \times 13\ mm^2$ was fixed in front of the ERD detector creating a solid angle of 2.6 msr. A 4 mm circular collimator was placed in front of the RBS detector delimiting a 1.9 msr solid angle.

Besides the isotopic purity, another important point to determine is the hydrogen depth profile. This can be measured using resonant nuclear reaction analyses (RNRA) such as the widely used $^1H(^{15}N,\alpha\gamma)^{12}C$ reaction showing a narrow and intense resonance at 6385 keV [34]. The depth profile is measured by varying step by step the incident energy of $^{15}N^{3+}$ from the resonant energy to the energy for which resonance arises at the end of the hydrogen distribution. At each energy, gamma rays of 4.438 MeV, produced by de-excitation of the $^{12}C$ nuclei, were counted in a NaI(Tl) well ($4'' \times 4''$). The target was placed in the well providing a nearly $4\pi$ steradian solid angle for gamma detection as shown in Fig. 4. To reduce build up on the sample, a liquid nitrogen cold trap was placed just in front of the target.

The advantage of RNRA is the narrow resonance exhibited by the cross-section allowing us to obtain hydrogen depth profiles with an excellent depth resolution. Furthermore, this technique was also used as a probe to study the stability of hydrogen at a chosen depth (at the maximum of the hydrogen concentration) as a function of the

[3] Passivated Implanted Planar Silicon.

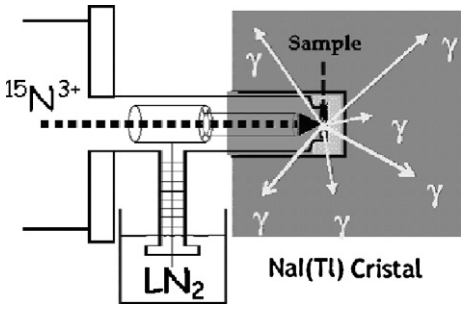


Fig. 4. Geometry used for RNRA experiments: the NaI(Tl) well surrounds the sample containing hydrogen. The $^{15}N^{3+}$ beam irradiates the target after passing through a liquid nitrogen cold trap to reduce contamination of the specimen.

$^{15}N$ ion fluence. The acquisition software used in these measurements allowed knowledge of the number of gamma rays detected for a given time range, continuously during data collection. Hence, any desorption could be observed. On the other hand, ERDA is sensitive to all hydrogen isotopes simultaneously and is used to verify the isotopic purity of the different samples. Thus, these two complementary analysis techniques were combined for sample characterization.

### 2.3. Cross-section measurement of the $^1H(^{13}C,\gamma)^{14}N$ reaction

To study the proton capture by incident $^{13}C$ nuclei, a more precise energy resolution detector sensitive to emitted gamma rays is needed. Thus a $3'' \times 3''$ Ge detector with a 2.2 keV resolution (for the detection of 661.6 keV gamma rays from $^{137}Cs$) was used. It was placed at 90° relative to the beam direction to minimize the Doppler effect on detected gamma rays. The distance from the target varied from 1 to 10 cm during the investigations, providing solid angles in the range of about 0.41–4.7 sr. Because of the long duration of some measurements, we used water cooling for the target during irradiation.

Usually, a resonance is measured by irradiating foils thicker than the hydrogen profile used in this investigation, with energy higher than the resonance energy, allowing all the resonance to be covered. In this work, the resonant cross-section was obtained by varying the beam energy from around 6.6–8.0 MeV in 100 keV steps. This energy step also corresponds to the energy loss by the $^{13}C$ in the hydrogen standard (silicon implanted hydrogen sample). Our method is more precise thanks to the energy precision of the ALTAÏS accelerator but it is time consuming. The data points given in the results of section 4 were obtained with a 0.3 mC electrical charge of $^{13}C^{3+}$ and beam currents ranging from 1 to 1.5 μA, which corresponds to $6.2 \times 10^{12}$–$9.4 \times 10^{12}$ part $s^{-1}$. The yield is the integration of gamma rays coming only from the radiative transition from the resonant to the fundamental levels. This corresponds to a region of interest including the 8.062 MeV photoelectric peak, its two escapes and the Compton background.

## 3. Results and discussion

### 3.1. Influence of implanted deuterium

First, implantations of hydrogen and deuterium were carried out separately by use of the ExB implanter. The goals were, on the one hand, to obtain samples with only hydrogen and no deuterium, and, on the other hand, to have a target containing a given quantity of deuterium. The latter is necessary to study the reactions that can be induced by this isotope. However, it appeared that the samples obtained by hydrogen implantation exhibited a large amount of deuterium, more than four times the natural concentration. This information was obtained with ERDA where, in addition to hydrogen, a signal was detected at higher energies, corresponding to the presence of deuterium in the bulk (Fig. 5(a)). The same analysis on a sample in which no deuterium is implanted (implanted with magnetic field separation) is given in Fig. 5(b) for comparison. Traces of deuterium were detected at the surface, due to contamination (probably due to water adsorption).

In fact, a Wien filter can separate two different ions only within a given energy window [35]. At low energies (below ~5 keV), the relative energy spread is too large and, hydrogen ($^1H^+$) and deuterium ($^2D^+$) cannot be discriminated. In a second step, the presence of deuterium in samples implanted with hydrogen by means of the magnetic separation implanter was investigated. The isotopic purity was reached and consequently all other implantations were carried out with this implanter. It is worth remembering that the cross-section of (d,p) [36] or (d,n) reactions is generally higher than (p,γ) reactions. In order to illustrate the importance of the isotopic purity, two silicon samples were implanted with hydrogen ($^1H$ only) and deuterium, respectively, and irradiated with a 7.2 MeV $^{13}C^{3+}$ beam. The detected gamma rays induced by the reaction have been plotted in Fig. 6. It is clearly observed that there is ~10 times more gamma rays detected in the case of the deuterium target, in spite of the smallest integrated charge (~10 times lower) meaning that the normalized background is 100 times larger for the sample implanted with deuterium. The detection parameters were nearly the same as those for $^{13}C(p,\gamma)^{14}N$ resonant cross-section measurement.

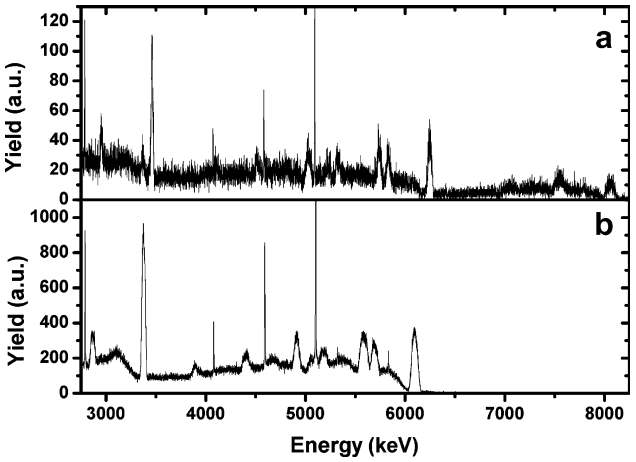


Fig. 6. Gamma spectrum obtained with $^{13}C^{3+}$ beam on targets of silicon implanted with hydrogen (a) and deuterium (b) for an integrated charge of 23.2 mC (a) and 2.5 mC (b).

### 3.2. Study of the retained dose

Having overcome the issue of isotopic purity, the next part of the study regards the evolution of the retained hydrogen dose with the implantation fluence. Fig. 7 shows the retained hydrogen dose as a function of the incident $^1H_2^+$ fluence. For an ion fluence lower than $6\times10^{16}$ at/cm$^2$, the retained dose increases linearly with a coefficient lower than 1 ($0.89\pm0.07$). A 'pseudo-saturation' is then

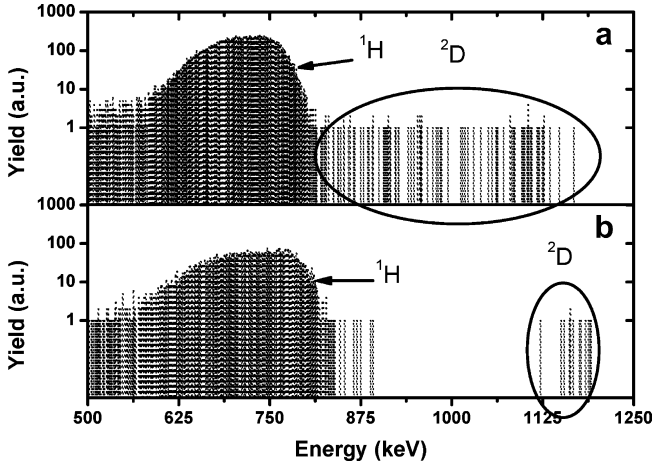


Fig. 5. Recoil spectrum at 20° of hydrogen and deuterium produced by alpha particles of 2.128 MeV irradiating samples implanted with hydrogen and deuterium (a) and presenting deuterium only on the surface (b).

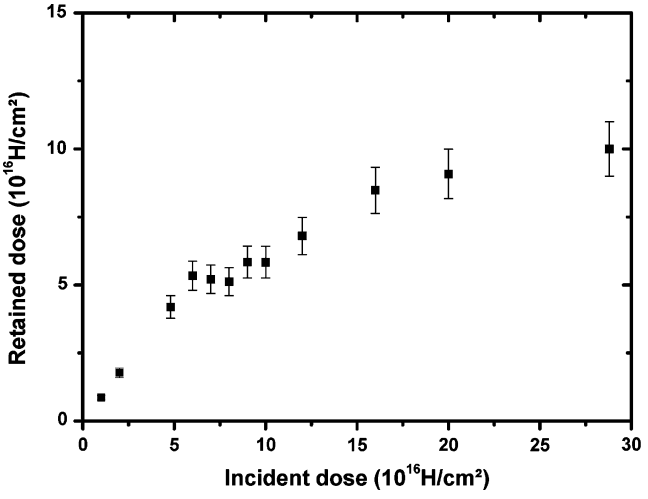


Fig. 7. Retained dose of hydrogen as a function of incident hydrogen fluence (3 keV $^1H_2^+$) in silicon. These values were obtained by means of alpha particles inducing hydrogen recoil.

observed, suggesting that silicon cannot contain more hydrogen than 6–7 × $10^{16}$ H/cm$^2$ up to a fluence of 1 × $10^{17}$ at/cm$^2$ (note the higher number of data points in this region). Beyond this fluence value, the retained dose increases again but reaches saturation at a dose of about 1 × $10^{17}$ H/cm$^2$.

The sputtering of implanted hydrogen may explain the fact that all the implanted hydrogen is not retained for fluences lower than 6 × $10^{16}$ at/cm$^2$. But a rough estimation establishes this value to less than 1% that is insufficient. Another possibility is the fact that a certain percentage of ions is backscattered from the target during implantation. Theoretical simulations with SRIM indicate 11.9% that corresponds to the lack of hydrogen measured after implantations.

Concerning the 'pseudo-saturation', we have already mentioned that hydrogen ions bind strongly with the silicon vacancies and H-terminates internal Si(1 0 0) surfaces; thus, an increasing quantity of defects has to be created for trapping of implanted hydrogen ions. From an ion fluence of 6 × $10^{16}$ H/cm$^2$, it seems that implanted hydrogen cannot find enough dangling bonds in the matrix to allow any binding with silicon. $H^+$ ions recombine themselves to form gaseous hydrogen that can diffuse to the surface and hence the quantity of hydrogen in silicon increases only slightly or remains constant. This occurs until the incident ions can create sufficient defects (possibly second generation) and thus can be trapped, compensating and stopping the escape of $H_2$. The retained dose increases again until final saturation around 1 × $10^{17}$ H/cm$^2$ for an incident ion fluence higher than 3 × $10^{17}$ H/cm$^2$. Regarding these results, a detailed study of the phenomena involved would be very useful. More, the dependency with some experimental conditions such as implantation temperature or implantation energy should be investigated.

### 3.3. Hydrogen standard properties

Two different implantation energies were carried out in samples to obtain a flat hydrogen distribution from the surface to a depth of ~100 nm, the convolution of two Gaussians being a rectangle. The fluences were chosen by taking into account the retained dose results and the data concerning blistering effects as discussed in [37]. This phenomenon would be very annoying. Indeed, blisters that contain gaseous hydrogen can flake if temperature increases and there is therefore a loss of hydrogen in the sample. Then, the desired profile was achieved with a first implantation at 3 keV to a fluence of 1 × $10^{17}$ $^1H^+$/cm$^2$ followed by a second at 1.5 keV to a fluence of 6 × $10^{16}$ $^1H^+$/cm$^2$. Five samples were obtained with this procedure and used for the verification of the standard reproducibility. The depth profiles, measured with ERDA and RNRA techniques are shown in Fig. 8. As desired, a 100 nm hydrogen distribution with a concentration reaching 18.5% has been obtained. Note that the depth resolution is better with RNRA because of the very small resonance width and

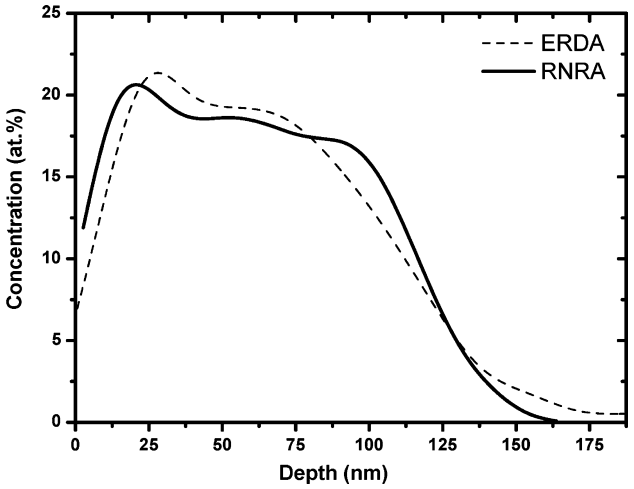


Fig. 8. Comparison of the depth profile of one sample implanted at two different energies and fluences (1 × $10^{17}$ $^1H^+$/cm$^2$ at 3 keV and 6 × $10^{16}$ $^1H^+$/cm$^2$ at 1.5 keV), obtained by ERDA (dashed line) with alpha particles and RNRA (straight line) with $^{15}N$.

the lower resolution in ERDA due to multiple collisions, as mentioned by Wielunski et al. [38]. In addition, the RNRA technique can differentiate the bulk and the surface contributions that do not have the same stopping power.

The good reproducibility of this type of sample can be seen in Fig. 9. It is worth noting that the surface contribution of hydrogen due to water adsorption and hydrocarbon contamination on the sample, coming from residual vacuum, is observed on the hydrogen depth profiles (Fig. 8). The surface contamination has been removed from the $^1H(^{15}N,\alpha\gamma)^{12}C$ energy spectra before deconvolution and only the bulk contribution is shown in Fig. 9. A retained ion dose of about 9 × $10^{16}$ $^1$H/cm$^2$ has been measured, confirming that a given amount of the implanted hydrogen has not been retained in the silicon matrix.

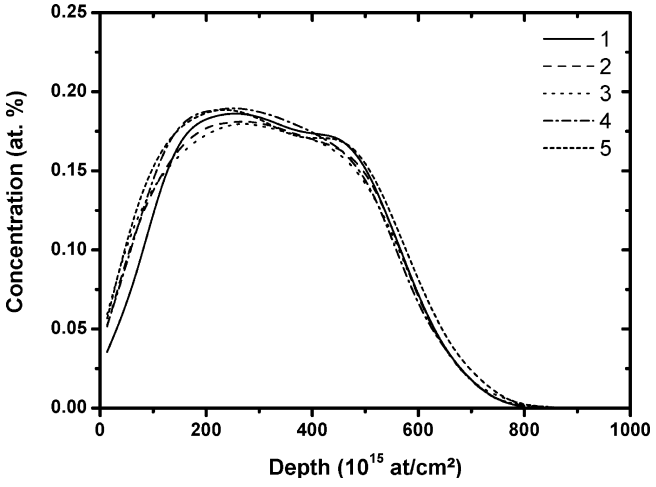


Fig. 9. Depth profiles of five samples implanted with two different energies and fluences (1 × $10^{17}$ $^1H^+$/cm$^2$ at 3 keV and 6 × $10^{16}$ $^1H^+$/cm$^2$ at 1.5 keV), obtained with RNRA after subtraction of the surface contamination peak.

Some properties must be controlled in order to obtain a reliable hydrogen standard. Reproducibility of the hydrogen depth profile has been observed. During the analyses of recoils, no deuterium was detected in the implanted region (but, as expected, it was detected in the surface contamination). The last point concerns the stability of hydrogen under ion irradiation. For this purpose, two investigations were done. First, some samples were carried out by implanting hydrogen ions in silicon with the SAMES implanter at LARN. The implantation energy was 24 keV, providing a hydrogen bulk distribution well discriminated from the surface contribution. Then, these samples were irradiated with $^{15}N^{3+}$ and the resonance of the $^{1}H(^{15}N,\alpha\gamma)^{12}C$ reaction was used to probe the surface ($E_{15_N} = 6385$ keV) and the bulk ($E_{15_N} = 6900$ keV) contributions separately. The number of gamma rays detected for each nano-coulomb of incoming ions as a function of time gives the evolution of the hydrogen distribution for different irradiating ion fluences. All points were obtained by integrating gamma rays of $^{12}C$ detected in the NaI(Tl) well. As shown in Fig. 10, a given quantity of hydrogen desorption has been observed at the surface. This can be fitted with a two-term inverse exponential curve, as suggested in [24]. This means that the hydrogen adsorbed at the surface quickly decreases at the beginning of irradiation and then stabilizes progressively. But for the implanted hydrogen, the evolution can be fitted with a straight line with zero-slope, which means that implanted hydrogen is stable for around 30 min. of irradiation for a total fluence of $2.4 \times 10^{14}$ $^{15}N^{3+}$ (Fig. 10).

A second investigation was performed to push the limits of irradiation even further. It consisted of measuring the hydrogen profile of a sample before and after a longer $^{13}C^{3+}$ irradiation (around 4.5 h) without atmospheric exposure between the different steps. The depth profile was obtained with RNRA by use of a $^{15}N$ beam. The beam switch was easily achieved thanks to the LARN accelerator. Because of the long irradiation, water cooling of the copper target holder was used to minimize sample warming. It appears that with an irradiation of more than $3 \times 10^{16}$ ions/cm$^2$, the implanted hydrogen profile remains unchanged. After deconvolution, two similar depth profiles were obtained.

Consequently, taking into account all of the above mentioned characterizations and observations, we can conclude that the samples obtained can be considered as hydrogen standards. The following section of this work aims at validating this type of standard by measuring a resonant cross-section. The details are given below.

## 4. Astrophysical application

The experimental data points obtained in reverse kinematics by using the developed hydrogen standards described above as target are shown in Fig. 11. Different characteristic values were obtained for this resonance, including the resonance energy and its width; these values are given in Table 1. The strength of the resonance accounts for the magnitude of the resonance. It can be seen in Table 1 that all values are in relatively good agreement with the ones published by King et al. [19], Ajzenberg-Selove [17] and the average values of Galster et al. [16] taking into account their measurements and some previous publications. This confirms the validity of the hydrogen standards.

The resonance energy and its width were obtained by means of a numerical simulation taking into account the convolution between the beam and the target thickness. A least squares method was applied to determine the parameters of the cross-section reproducing the experimental yield. We used the Breit–Wigner equation [39] that takes into account the energy dependency of the width thanks to the penetration factor. The calculated experimental yield is also shown in Fig. 11 (solid line). The resonance energy and

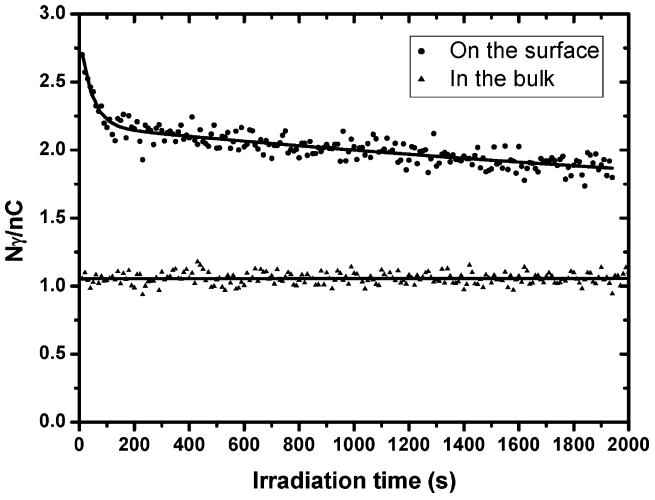


Fig. 10. Desorption of surface hydrogen fitted with a two-term inverse exponential curve and stability of implanted hydrogen, during irradiation of $^{15}N$.

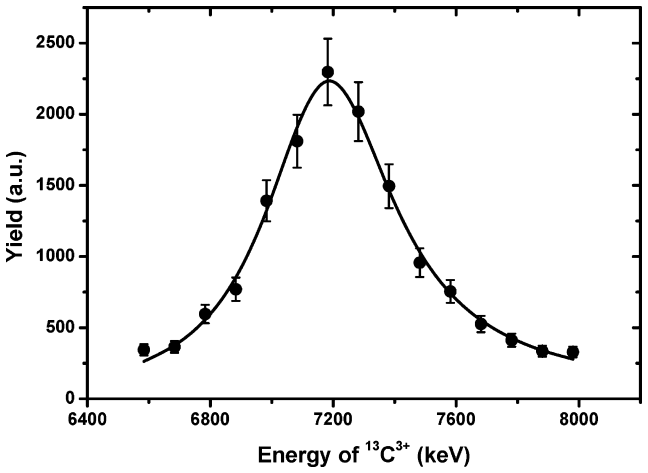


Fig. 11. Resonant cross-section of $^{13}C(p,\gamma)^{14}N$ measured in reverse kinematics: Experimental yield (dots) with the least squares fit (solid line).

Table 1
Interesting values (in the CM system) for the 511 keV resonance of $^{13}C(p,\gamma)^{14}N$

| Source | Resonance energy (keV) | Resonance width (keV) | Strength (eV) |
|---|---|---|---|
| This work | $511.5 \pm 0.2$ | $36.9 \pm 0.5$ | $7.0 \pm 0.8$[a] $9.2 \pm 1.2$[b] |
| King et al. [19] | $517.8 \pm 0.5$ | $37 \pm 1$ | $8.8 \pm 1.1$ |
| Ajzenberg-Selove [17] | $512 \pm 1$ | $23 \pm 1$ | 9.2 |
| Galster et al. [16] | $511.5 \pm 1.2$ | $33.8 \pm 1.2$ | $8.5 \pm 1.2$ |

[a] Obtained with [19].
[b] Obtained with [16].

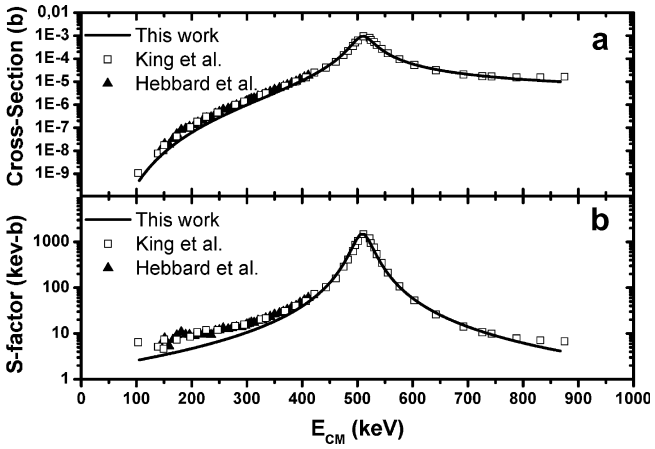


Fig. 12. Comparison between the cross-section (a) and S-factor (b) values of King et al. [19], Hebbard et al. [40] and our normalized measurement that is extrapolated.

the width in Table 1 are those corresponding to the Breit–Wigner function providing the best fit of the experimental data. In Fig. 12(a), the solid line gives an extrapolation of this suitable function in the center of mass system, which is the cross-section. An absolute value is given by normalizing our data with the results of King et al. [19]. In order to compare our results with the previous measurements, the values for the cross-section taken in King et al. and in Hebbard and Vogl [40] are added. These are references used in NACRE [18], as it is visible in Fig. 2. The cross-sections from [19] and from this work are nearly superposed for energies in the range of ~450–725 keV, when our measurements cover an energy range of around 470–570 keV. It is a good result but precise measurements at lower (and higher) energies are required. The Fig. 12(b) shows the S-factors corresponding to the cross-sections of Fig. 12(a). The energy dependant S-factor $S(E)$ is defined from the reaction cross-section $\sigma(E)$ as follows:

$$\sigma(E) = \frac{1}{E}\exp(-2\pi\eta)S(E) \tag{1}$$

with $\eta$ the Sommerfeld parameter. $S(E)$ is a value that includes only the nuclear contribution of the cross-section and is therefore the most relevant value for astrophysics considerations. Regarding the Fig. 12, particularly the Fig. 12(b), the need of measurements at low energies, where the extrapolation does not agree with the other values, is reinforced.

The values obtained for the resonance energy and its width $\Gamma$ allowed us the calculation of the resonance strength $\omega\gamma$, as given in Table 1. We used the following formula:

$$\sigma_r = 4\lambda_r^2 \frac{\omega\gamma}{\Gamma} \tag{2}$$

This is the total cross-section at the resonance energy, depending of the de Broglie wavelength at the resonance, $\lambda_r$. To obtain $\omega\gamma$, it is necessary to measure the cross-section. We first used the value of [19] which was already exploited for the normalization. Secondly, the cross-section obtained with the mean parameters of [16] introduced in formula (2) was used.

We can discuss the different values obtained. Concerning the resonance energy, our value of $511.5 \pm 0.2$ keV is close to those of literature, except the $517.8 \pm 0.5$ keV. In [16], nearly all of their measurements are in the range of 509–512 keV. For the resonance width, $36.9 \pm 0.5$ keV is rather high compared to the average value given by Galster et al. but is close to the $37 \pm 1$ keV of King et al. The $23 \pm 1$ keV coming from [23] is dramatically low, as mentioned in [16]. Interestingly, the more recent values are usually higher. Finally, the resonance strength gives a range of 7–9.2 eV, depending of the cross-section. We are currently developing an experimental setup to allow the measurement of this absolute cross-section. Regarding the resonance strengths, it seems that this value is closer than the one calculated from Galster et al. ($1.24 \pm 0.18$ mb) parameters, comparatively to the one of King et al. ($0.94 \pm 0.11$ mb).

In addition, the cross-section at a lower energy corresponding to about 355 keV in the center of mass system has been measured. The value obtained, though needing confirmation by more precise and systematic measurements, gives confidence for future investigations of this reaction for stellar energies. The most interesting ones are in the range of 79–190 keV (Gamow window for a temperature of $2 \times 10^8$ K), which corresponds to 1.106–2.660 MeV in reverse kinematics.

## 5. Conclusions and prospects

A hydrogen standard was developed by means of ion implantation of $^1H^+$ in silicon. Ion implantation was performed for two different implantation energies and fluences in order to obtain a flat hydrogen depth profile from the

surface to a depth of about 100 nm, neglecting surface contamination. The absence of deuterium in the implanted hydrogen was controlled, thus establishing that the necessary isotopic purity of the standard (nearly 100%) has been mastered. For future investigations, measurements will be performed in ultra high vacuum to control the surface contamination.

Sample reproducibility was also verified. Moreover, the evolution of hydrogen during ion irradiation was investigated. It appeared that, contrary to the hydrogen adsorbed at the surface that suffers from ion induce desorption, the implanted hydrogen was stable under irradiation. This is attributed to the strong binding of hydrogen ions in silicon.

Finally, the hydrogen standard was validated by measuring a resonant cross-section of a nuclear reaction involved in nucleosynthesis that takes place in stars. The results indicate that this type of target constitutes a reliable hydrogen standard for work in reverse kinematics on nuclear reactions of astrophysical interest. But this standard can also be used for the determination of the cross-section of any reaction involving a proton, occurring in stars or not.

## Acknowledgments

G. Genard was supported as research fellow by the Belgian Fund for Scientific Research (F.R.S.-FNRS) and M. Yedji by the Natural Science and Engineering Research Council of Canada (NSERC). This work was achieved within the SC-TEC-02 collaboration between the Wallonie-Bruxelles Community and the Québec government. We acknowledge P. Leleux from UCL (Belgium) for supplying us the Ge detector.

## References

[1] R. Gibala, R.F. Hehemann, Hydrogen Embrittlement and Stress Corrosion Cracking, American Society for Metals, 1992.
[2] M. Bruel, Nucl. Instr. and Meth. B 108 (1996) 313.
[3] C. Maleville, B. Aspar, T. Poumeyrol, H. Moriceau, M. Bruel, A.J. Auberton-Herve, T. Barge, Mater. Sci. Eng. B 46 (1997) 14.
[4] X.Q. Feng, Y. Huang, Int. J. Solids Struct. 41 (2004) 4299.
[5] M. Xu, X.Q. Feng, Theor. Appl. Fract. Mech. 42 (2004) 295.
[6] Y.Q. Wang, R. Smirani, G.G. Ross, Physica E 27 (2004) 97.
[7] G. Terwagne, D.D. Cohen, G.A. Collins, Nucl. Instr. and Meth. B 84 (1994) 415.
[8] G. Terwagne, G. Deconninck, Nucl. Instr. and Meth. B 64 (1992) 153.
[9] G. Terwagne, G.G. Ross, L. Leblanc, J. Appl. Phys. 79 (1996) 8886.
[10] V.F. Kharchenko, M.A. Navrotski, P.A. Katerinchuk, Nucl. Phys. A 552 (1993) 378.
[11] H.A. Bethe, Phys. Rev. 55 (1939) 103 & 434.
[12] W.A.S. Lamb, R.E. Hester, Phys. Rev. 108 (1957) 1304.
[13] A. Formicola et al., Phys. Lett. B 591 (2004) 61.
[14] R.C. Runkle, A.E. Champagne, C. Angulo, C. Fox, C. Iliadis, R. Longland, J. Pollanen, Phys. Rev. Lett. 94 (2005) 082503.
[15] A. Lemut et al., Phys. Lett. B 634 (2006) 483.
[16] W. Galster et al., Phys. Rev. C 44 (1991) 2776.
[17] F. Ajzenberg-Selove, Nucl. Phys. A 449 (1986) 1.
[18] C. Angulo et al., Nucl. Phys. A 656 (1999) 3.
[19] J.D. King, R.E. Azuma, J.B. Vise, J. Görres, C. Rolfs, H.P. Trautvetter, A.E. Vlieks, Nucl. Phys. A 567 (1994) 354.
[20] J.D. Seagrave, Phys. Rev. 85 (1952) 85.
[21] D.F. Hebbard, Ph.D. thesis, University of Melbourne, 1957.
[22] E.A. Milne, Phys. Rev. 93 (1954) 762.
[23] R.A. Spits, W. Baloyi, T.E. Derry, Phys. Rev. C 41 (1990) 2429.
[24] G.G. Ross, I. Richard, Nucl. Instr. and Meth. B 64 (1992) 603.
[25] F. Schiettekatte, G.G. Ross, A. Chevarier, N. Chevarier, A. Plantier, Nucl. Instr. and Meth. B 132 (1997) 607.
[26] O. Moutanabbir, B. Terreault, M. Chicoine, F. Schiettekatte, Appl. Phys. A 80 (2004) 1455.
[27] Y.J. Chabal, M.K. Weldon, Y. Caudano, B.B. Stefanov, K. Raghavachari, Physica B 273–274 (1999) 152.
[28] S.K. Estreicher, J.L. Hastings, P.A. Fedders, Phys. Rev. B 57 (1998) 20.
[29] E.J. Evers, F.H.P.M. Habraker, Spectroc. Acta Pt. B 139 (1984) 1553.
[30] M. Hrmacher, M. Schwickert, H. Schebela, K.P. Lieb, J. Alloy. Compd. 404 (2005) 307.
[31] G.G. Ross, L. Leblanc, Nucl. Instr. and Meth. B 62 (1992) 484.
[32] J.F. Ziegler, J.P. Biersack, SRIM (2003).
[33] V. Quillet, F. Abel, M. Schott, Nucl. Instr. and Meth. B 83 (1993) 47.
[34] K.M. Horn, W.A. Lanford, Nucl. Instr. and Meth. B 34 (1988) 1.
[35] J. Tirira, Y. Serruys, P. Trocellier, Forward Recoil Spectrometry – Applications of Hydrogen Determination in Solids, Plenum Press, 1996, 163.
[36] J.L. Colaux, T. Thome, G. Terwagne, Nucl. Instr. and Meth. B 254 (2007) 25.
[37] A. Giguere, B. Terreault, G. Genard, G. Terwagne, J. Appl. Phys., submitted for publication.
[38] L.S. Wielunski, D. Grambole, U. Kreissig, R. Grötzschel, G. Harding, E. Szilágyi, Nucl. Instr. and Meth. B 190 (2002) 693.
[39] G. Breit, E. Wigner, Phys. Rev. 49 (1936) 7.
[40] D.F. Hebbard, J.L. Vogl, Nucl. Phys. 21 (1960) 652.